Drug Mimetic Organogelators for the Control of Concomitant Crystallization of Barbital and Thalidomide

Basanta Saikia,[a] Matthew T. Mulvee,[b] Ivan Torres Moya,[c] Bipul Sarma,[a] Jonathan W. Steed[b]**

[a] Department of Chemical Sciences, Tezpur University, Napaam-784028, Assam, India

[b] Department of Chemistry, Durham University, South Road, Durham, DH1 3LE, UK

[c] Department of Organic Chemistry, University of Castilla La Mancha, 13071 Ciudad Real, Spain.

E-mail: [a] bcsarma@tezu.ernet.in, [b] jon.steed@durham.ac.uk

Keywords: Concomitant polymorphism, Organogelators, Bis(urea), Gel phase crystallization, Barbiturates

Abstract

A strategic approach to control the polymorphism of two related drugs by introducing a drug-mimetic imide functional group into the molecular weight organogelator structure is presented. This was achieved with novel aminoglutethimide-derived bis(urea) organogelators designed to form gels that act as targeted crystallization media for (±)-thalidomide and barbital. The organogelators prevent concomitant crystallization, a serious issue for drug formulation and development. This work demonstrates the potential to control concomitant crystallization with rationally designed supramolecular gelators.

Introduction

Supramolecular gels are formed through the self-assembly of gelators (typically at low concentrations *i.e.* <2% by mass) into filaments which entangle and branch to form a three-dimensional network that immobilizes the solvent to produce a viscoelastic material.[1–5] These gelators can be relatively straightforward to synthesize and functionalize, with potential applications in catalysis, biomedical research, drug delivery and pharmaceutical crystallization.[6–11] Bis(urea) gelators, in particular, can be synthetically modified to design gelators with desired functionalities and specific properties while retaining their gel-forming ability.[12] Generally, bis(urea) gels are thermally reversible as they are formed through reversible non-covalent interactions and their gelation behavior can be manipulated by altering the experimental conditions.[2,13–15] Furthermore, the prevention of convection effects, reduced solvent evaporation rate and the possibility of designing drug-specific binding functionality, means that supramolecular gels are emerging as effective media for pharmaceutical crystallization.[11,16,17]

Drug solid form screening, solid form control and crystal morphology are of key industrial significance.[18,19] Crystal form control has vital importance in the pharmaceutical development process as different crystal structures (polymorphs) or solvated forms (solvates) of the same drug exhibit different physiochemical properties such as solubility, tabletability, melting behavior, hydration stability, bulk density and bioavailability, which eventually impact on the overall drug efficacy.[18] In addition, factors like crystal morphology and particle size also need careful attention as they can influence the drug physiochemical, formulation and processing properties.[20] Moreover, a thorough understanding of the solid forms landscape can represent intellectual property opportunities.[21] Nucleation events and crystal growth can be guided at interfaces by molecular recognition. Crystallization using heterogeneous surfaces such as a self-assembled monolayer (SAM),[19] or a polymer additive and techniques like laser-induced crystallization,[22] are also being

44 incorporated into pharmaceutical screening and solid form control and discovery methods.[23] New
45 crystallization methods such as nanoconfinement, nanodroplet crystallization,[24] the use of tailored
46 additives[25,26] and careful temperature control[27] are significantly expanding solid form landscapes.
47 Bora *et al.* recently reported that crystallization on functionalized SAM surface could effectively
48 control concomitant nucleation of flexible molecules.[19]

49 Recent work has demonstrated the feasibility of gel-phase crystallization to control crystal size,
50 morphology and polymorphic outcome.[11,16,28,29] It has been proposed that the gel fibers can act as
51 a surface for templated nucleation of active pharmaceutical ingredients (APIs). Different solid-
52 state crystal forms (polymorphs) can differ in lattice energy by only a few kJ mol^{-1} [30,31] and so the
53 presence of the gel fiber surface can bias the system towards the crystallization of a particular
54 form.[32] Depending on the gel-solute interactions, gels offer the possibility of obtaining new forms
55 or metastable solid forms that are not be obtainable from the conventional crystallization
56 methods.[11,17] Functionalized gels can offer potential alternate nucleation sites and hence can
57 influence the crystallization outcome. Polymorphic control of the highly polymorphic molecule
58 ROY has been demonstrated by utilizing a rationally designed organogel as the crystallization
59 medium.[16] Other modifications of crystal properties such as size, morphology, and change in
60 polymorphism in gel phase crystallization have been reported.[11,16,17,29,33]

61 While often the discovery of gelators is serendipitous, bis(urea)s are prone to form gels in the
62 presence of a wide variety of terminal substituents as they often aggregate *via* one-dimensional
63 hydrogen bonding to form highly anisotropic morphologies that are commonly linked to
64 gelation.[4,12] As the urea groups are expected to be involved in urea α-tape like hydrogen bonding
65 it is possible to append drug-mimetic functional groups at the periphery of the gelator that are
66 available to interact with the API solute and hence influence its crystallization.

67 Despite its notorious history, (±)-thalidomide (THL) has attracted considerable clinical interest
68 in recent years due to its unique pharmacological effect against several diseases, especially
69 cancer.[34] Racemic THL has two known solid forms, termed α and β.[35] Barbital (BAR) was the
70 first commercially available barbiturate and is a well-known sedative.[36] It is highly polymorphic
71 with six known non-solvated forms.[36] Crystal structures of three polymorphs of BAR *i.e.* forms I,
72 III and V have been reported, which exhibit packing polymorphism, and are known to crystallize
73 concomitantly (Scheme 1).[36,37] Concomitant polymorphism involves the crystallization of
74 different forms, from the same crystallization batch and it is common when the crystal packing
75 energy differences between forms are relatively insignificant.[19,38,39] However, formulation of a
76 pure single form of a drug is crucial in the pharmaceutical industry since varying amounts of
77 different polymorphs can give rise to an inconsistent product profile and performance. Therefore
78 attaining control over concomitant polymorphism as observed for BAR is essential from its
79 efficacy and formulation point of view.[40]
80 In this work, we have designed three new bis(urea)-based low molecular weight gelator
81 (LMWG) bearing the drug-mimetic imide group that occurs in important drug classes such as
82 barbiturates and thalidomide and its analogs to act as a potential site of interaction with the target
83 APIs (Scheme 2). We show that these targeted gelators achieve control over the concomitant
84 polymorphism of BAR and influence the outcome of THL crystallizations.

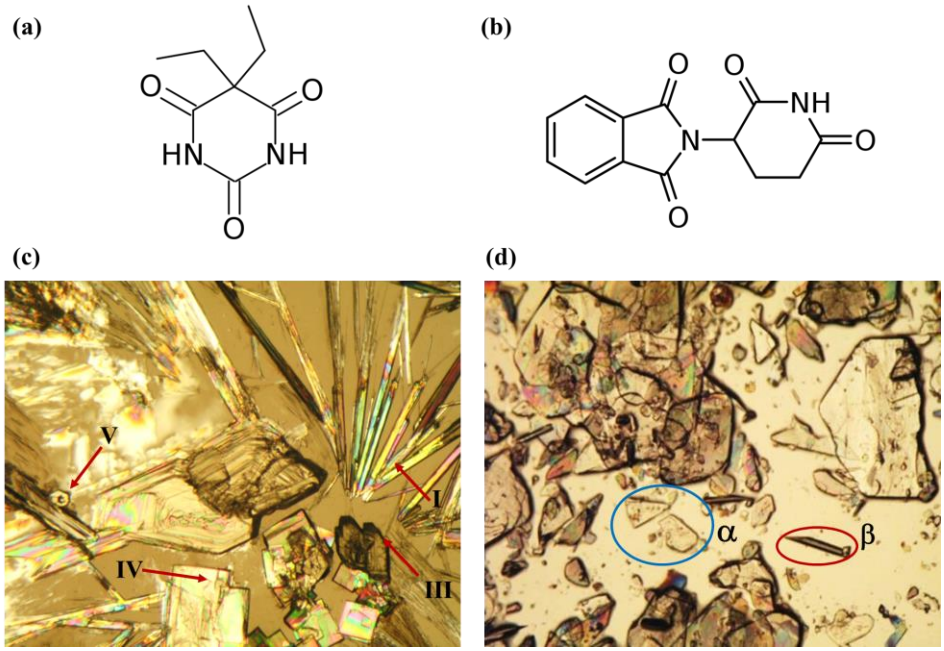

Scheme 1 Chemical structures of APIs (a) barbital (BAR) and (b) (±)-thalidomide (THL); concomitant polymorphism from solution crystallization of (c) BAR from cyclohexanone and (d) THL from nitromethane. Needle *β* form (red circle) and plate-shaped *α* form (blue circle) of THL.

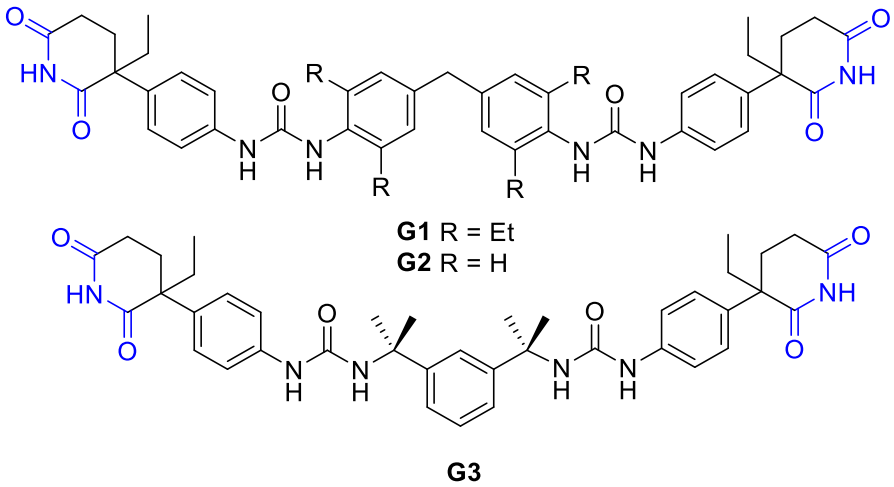

Scheme 2 Design of drug mimetic gelators **G1**–**3**, with the imide group shown in blue.

Results and Discussion

Synthesis

95 The three gelators (**G1** – **G3)** were synthesized in good yield using the commercially available
96 (±)-aminoglutethimide as the precursor and the appropriate diisocyanate (see Electronic
97 Supporting Information, Schemes S1 – S3). The gelators were characterized by nuclear magnetic
98 resonance (NMR) spectroscopy, Fourier-transform infrared (FTIR) spectroscopy, mass
99 spectrometry and elemental analysis (see ESI).
100
101 *Gel screening and Characterization*
102 Gel screening of **G1, G2 G3** was carried out using a wide range of solvents and solvent
103 combinations at 2 % (w/v) (Table 1). Samples were dissolved with gentle heating and sonication
104 until full dissolution. Gel formation was typically observed upon cooling to room temperature
105 within a few minutes though in some cases gelation took several hours. Gel formation was assessed
106 qualitatively by simple inversion of the sample vial. Gelator **G1** forms gels in 13 of the 29 solvents
107 and solvent combinations tested including some alcohols, cyclic ketones, 1,4-dioxane and nitro
108 compounds (See ESI Figure S4).
109 The low solubility of gelator **G1** prevents the formation of gels in most alcoholic solvents
110 such as methanol and 1-propanol. The addition of a few drops of DMSO readily dissolved the
111 gelator with further heating so that it forms gels in all the alcoholic solvents tested upon cooling.
112 The critical gelation concentration (CGC) for **G1** is typically 1.7 – 2 % (w/v) for alcoholic solvents,
113 while in the case of nitrobenzene, cyclohexanone, cyclopentanone, 1,4-dioxane, tetrahydrofuran a
114 lower CGC of 0.8 – 1 % (w/v) was observed. While **G1** is an effective gelator, **G2** and **G3** form
115 gels in only in two or three different solvents or solvent mixtures (Table 1). Gelator **G2** forms gels
116 in nitrobenzene and a 3:1 mixture of ethanol and cyclohexane (see ESI Figure S4b) with CGC of
117 0.8 and 0.9 % (w/v), respectively. **G3** gels nitrobenzene, nitromethane and a 2:1 toluene/ethyl

118 acetate mixture (see ESI Figure S4c) with a CGC of 0.8 % (w/v) in each case. All gels were either
119 translucent or opaque and became more opaque over time. This is commonly attributed to fibers
120 laterally associating to form larger bundles, which scatter light more, thus appearing more
121 opaque.[41,42] FT-IR analysis of the gels demonstrated a lowering of the IR frequency for
122 carboxamide peak (~1692 cm^{-1}) for the gels, which we attribute to intermolecular hydrogen
123 bonding between the gelator molecules (ESI Figure S5).
124
125 **Table 1** Gel screening results for **G1**, **G2** and **G3**, all at 2% (w/v).

Solvent	**G1**	**G2**	**G3**
1,2,4-trichlorobenzene	P	S	S
2-propanol	PG	PG	S
Acetone	P	S	S
Ethanol	G	PG	PG
Methanol	PG	PG	PG
Methanol+ DMSO	G	PG	PG
1-Pentanol	G	PG	PG
1,4-Butanediol	G	PG	PG
1-Propanol	PG	PG	PG
1-Propanol+ DMSO	G	PG	PG
1-Butanol	G	S	PG
2-Butanol	PG	IS	PG
2-Butanol+ DMSO	G	S	PG
Benzyl Alcohol	PG	S	S
Chloroform	IS	IS	IS
Dimethyl sulfoxide	S	S	S

Dimethylformamide	S	S	S
Ethyl Acetate	IS	IS	S
Nitrobenzene	G	G	G
Nitromethane	G*	PG	G
1,4-Dioxane	G	S	S
Tetrahydrofuran	G	S	S
Cyclohexanone	G	S	P
Cyclopentanone	G	P	P
Toluene	P	P	S
H_2O	P	S	S
EtOH: Cyclohexane (3:1)	PG	G	PG
Toluene: Ethyl acetate (2:1)	PG	PG	G

P= Precipitate, G= Gel, PG= Partial Gel, I= Insoluble with heating. * Very soft gel

The sol phase transition temperature, T_{gel}, was recorded by heating the gels and recording the temperature at which a small ball bearing fell through the sample, indicating disruption of the gel network.[43] Gels formed with **G1** were found to be generally quite stable with a T_{gel} of 97 °C at a concentration of 2% (w/v) for cyclohexanone (see ESI, Table S1). The gel of **G3** in nitromethane has a much lower T_{gel} of 45 °C at 2 % (w/v). In nitrobenzene and a mixture of toluene/ethyl acetate (2:1) the T_{gel} values for **G3** are 101 and 83 °C, respectively. The latter value is above the 77 °C boiling point of ethyl acetate and was evaluated in a sealed container. This relatively high T_{gel} suggests that gels of **G3** may be relatively robust.

Representative gels were characterized using oscillatory rheology. In all cases, the storage modulus (G') was at least an order of magnitude greater than the loss modulus (G''), indicative of the solid-like nature of the materials (Figure 1).[44,45] The mechanical properties of the gels were

relatively insensitive to the oscillation frequency, with G' higher than G'' in all cases, and they remain almost constant over the entire angular frequency range (ESI Figure S7), again typical behavior for supramolecular gels. Scanning electron microscopy (SEM) was used to image the morphology of the xerogels formed from **G1**, **G2** and **G3** a highly entangled network as observed for all samples (Figure 1b). The SEM sample of **G1** is obtained from drying a 2% (w/v %) gel in ethanol and shows a helical twisted morphology (Figure 1bi). A cylindrical ribbon type morphology is observed for a 1 % (w/v %) xerogel of **G2** obtained from nitrobenzene (Figure 1bii). A dense network of helical morphology is observed for 1 % (w/v %) xerogel of **G3** in nitromethane (Figure 1biii).

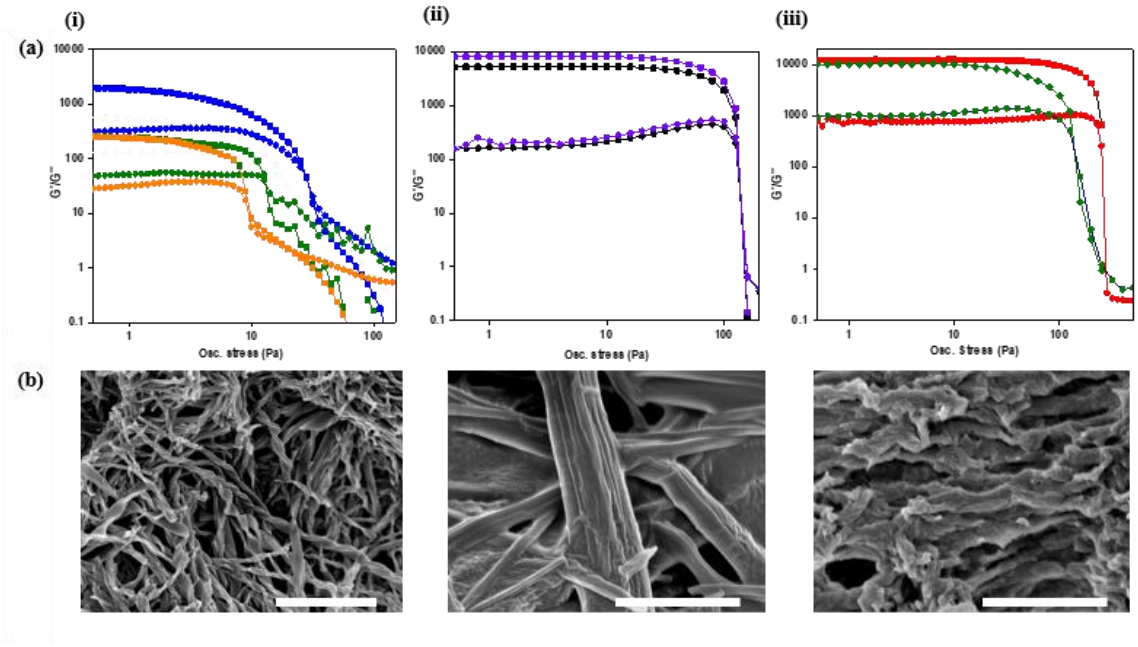

Figure 1 (a) Oscillatory stress sweeps at a constant frequency (1 Hz) (i) **G1**, (ii) **G2** and (iii) **G3**. (i) Cyclohexane (blue), nitrobenzene (green), butanol (orange); (ii) ethanol: cyclohexane 1% (w/v) (black), 2 % (w/v) (purple); (iii) nitromethane (red), toluene: ethyl acetate (2:1) (green). In all cases ■ refer to G′ (elastic moduli) and ● refer to G″ (viscous moduli). (b) SEM images of the xerogels (i) **G1**, (ii) **G2** and (iii) **G3** demonstrates the fibrous nature of the gels. (Scale bar: 2 μm)

Crystallization of Barbital

157 The UNI force-field introduced by Gavezzotti and Filippini[46,47] and implemented in the
158 Cambridge Crystallographic Data Centre Mercury package (Mercury 4.2.0)[48] was used to calculate
159 the relative packing energy of the BAR polymorphic forms based on the single-crystal structures
160 (DETBA01-12) deposited in the Cambridge Structural Database.[49] The packing energies are
161 comparable with packing energy –114.9, –118.2 and –119.5 kJ mol^{-1} for polymorphs I, III and V,
162 respectively. These similar packing energies are consistent with the observation of concomitant
163 polymorphism.
164
165 **Table 2** Comparison of crystallization outcome from solution and gel crystallization of barbital.

Solvent	**Solvent Crystallization**	**G1**	**G2**	**G3**
Ethanol	I, III, IV, V	III (prism), V	No gel	No gel
1-Butanol	I, III, V	III (rod)	No gel	No gel
1,4-Butane-diol	I, III, V	III (prism)	No gel	No gel
1-Pentanol	I, III, IV, V	III (prism)	No gel	No gel
Nitrobenzene	III	III	III	III
Nitromethane	III (needle)	III (prism)	No gel	Gel Unstable
Cyclohexanone	I, III, IV, V	III (prism)	No gel	No gel
Toluene/ethyl acetate (2:1)	III and V	No gel	III (prism)	No gel
EtOH/cyclohexane (3:1)	III and V	No gel	No gel	III (prism)

Solution crystallizations were performed by slow evaporation in a sealed vial with pinhole openings at room temperature. Crystallizations of barbital in the gels were carried out in parallel to solution crystallization, at 10% w/v.

166

167 The tendency of BAR to crystallize multiple forms concomitantly is well known and occurs in
168 many solvents (Table 2).[36,37] Similarly subliming BAR between 100 and 120°C results in the
169 concomitant crystallization of forms I, IV, V and III.[36] MacDonald *et al*. employed chemically
170 modified surfaces in microfluidic channels to control the nucleation of barbital polymorphs,
171 however, they were not able to control selectivity between forms I, III and IV at the surface of
172 SAMs.[37] Gel phase crystallizations of BAR were carried out in parallel to solution crystallization,
173 typically at 10% w/v and crystals typically formed in 3-4 days (see Experimental for details). The
174 crystals that were obtained from control solution crystallization from alcoholic solvents gave rise
175 to concomitant crystallization of polymorphs I, III, IV and V of BAR which were identified by
176 optical microscopy, single-crystal unit cell determination for at least five crystals, PXRD, DSC
177 and FT-IR analysis.[36] Form I and III proved to be more abundant by solvent crystallization and
178 occurred along with forms V and IV. However, form IV transform to Form I within 30 minutes
179 outside solvent at room temperature and demonstrated by FT-IR analysis (ESI, Figure S8). Under
180 the same experimental condition *i.e.* 100 mg/mL of barbital, gels of **G1** in 1-butanol (1.8 w/v %),
181 1-pentanol (1.8 w/v %), and 1,4-butanediol (1.8 w/v %), produced only the kinetic form III of
182 BAR. However, in the case of ethanol (1.7 w/v %) trace amount of crystals of another kinetic form,
183 form V was also observed along with polymorph III. In the case of nitrobenzene, no differences
184 between crystals obtained from the solution and gel phase crystallization were observed. This is
185 not surprising since the kinetic form is already favored in nitrobenzene. The solution crystallization
186 of BAR from nitromethane (10 w/v %) resulted in dense needle-shaped crystals (Figure 3aiii).
187 These crystals were analyzed by FTIR spectroscopy and unit cell determination and were found to
188 be a concomitant mixture of polymorphs III and V. However, nitromethane gels of **G1** (2 w/v %)
189 produced large prism-shaped crystals of polymorph III without the concomitant presence of Form

190 V. Thus, in contrast to solution crystallization methods, gel phase crystallization of BAR using the
191 gelator **G1** exhibits high selectivity for the kinetic form III polymorph. This selectivity is also
192 observed for gels formed using **G2** and **G3** in two different solvents implying that the common
193 imide on all the gelators plays major role in control the crystallization outcome. It is possible that
194 the interaction of the drug molecules with the gel fiber surface might increase the nucleation rate
195 of the kinetic form and thereby suppresses the nucleation of competing forms. A comparison
196 between gel phase and solution phase crystallization outcomes is shown in Figure 3. In the
197 presence of gelator in the gel state can alter the crystallization behavior of barbital and thereby
198 prevent the concomitant crystallization and confirmed the observations from PXRD, DSC, FT-IR
199 and SCXRD. These observations were further verified by conducting additional gel phase
200 crystallizations using previously reported gelators that do not contain the imide functionality; **G4**
201 contains nitro aryl groups,[16] and **G5** a salt gelator bearing carboxylate groups (Figure 2).[50] All
202 crystallizations in these gels failed to prevent concomitant polymorphism. This indicates that it the
203 imide functionality of the mimic gelators rather than the growth in a viscous gel network that
204 prevents concomitant crystallization either enhancing nucleation of Form III or, more likely,
205 suppressing nucleation of the other forms. Furthermore, quantitative analysis of the intermolecular
206 interactions for the different forms of BAR i.*e.* I, III and V were performed using Hirshfeld
207 surfaces and represented as 2D fingerprint plots (ESI Figure S10).[51] Significant differences were
208 observed for the different forms. Notably, the higher contribution of the O···H interactions in form
209 III (45%) compared to Form I and V (40.8% and 40.1%, respectively). Thus, it speculated that the
210 polar end groups of the mimetic gelators may be able to interact with the nuclei of Form III more
211 favorably and promote the growth due to a local supersaturation of this form over Form I or V.[52]

212 However, crystal growth mechanisms and the link between nuclei ordering and the final crystal

213 structure are not well understood, and is beyond the scope of this work.

214

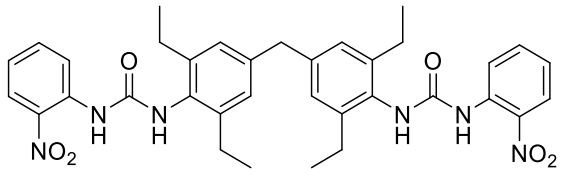

G4

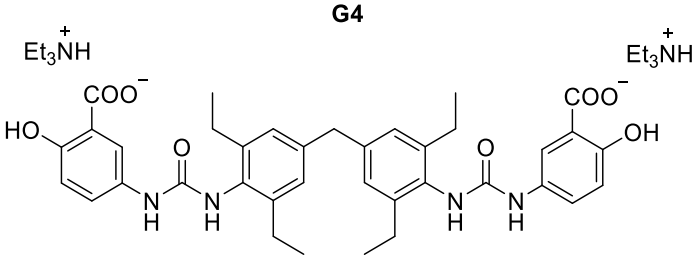

G5

215

216 **Figure 2** Chemical structures of control gelators **G4** and **G5** for the crystallization of BAR.

217

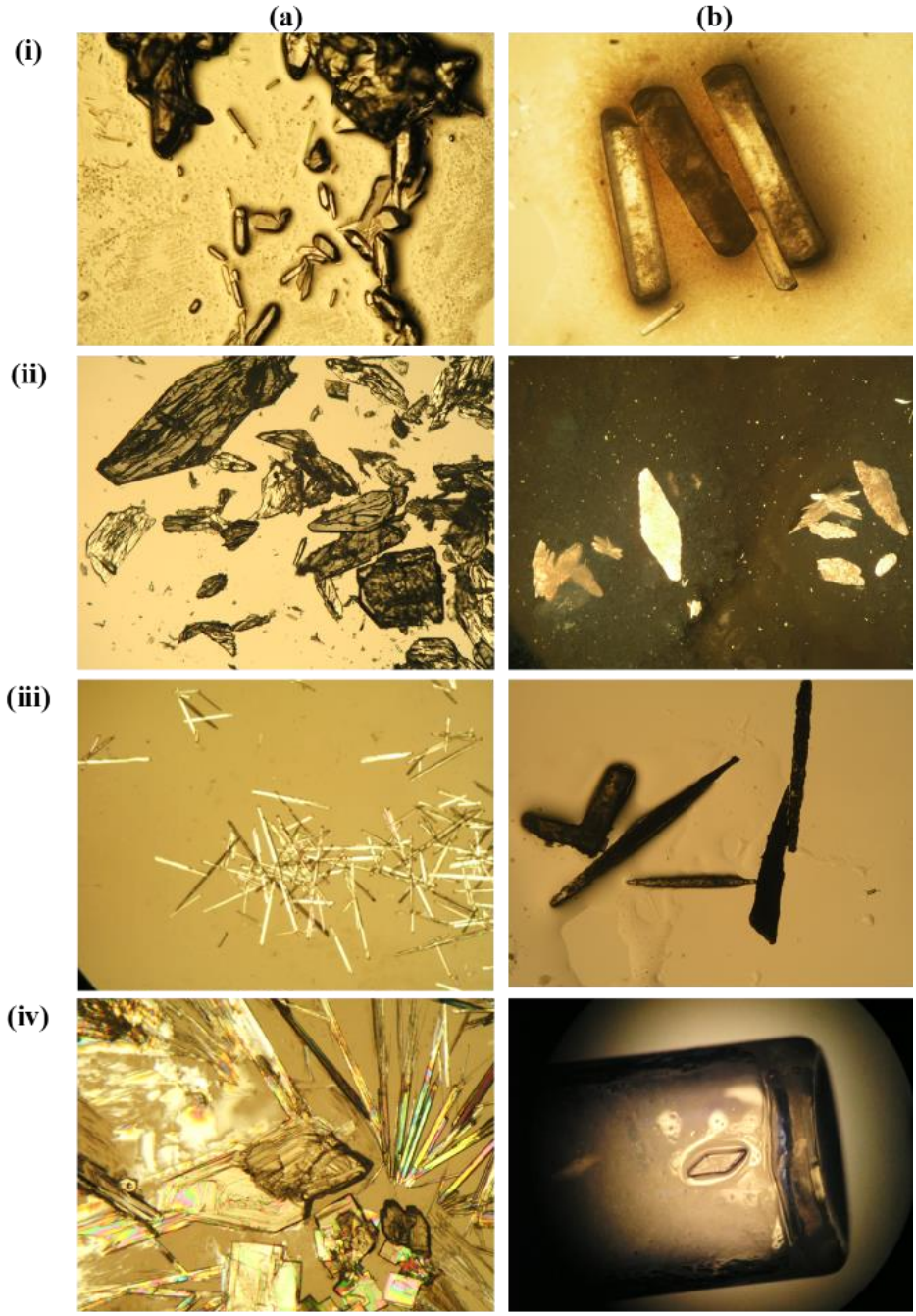

Figure 3 Photos of BAR crystals produced from (a) solution crystallizations and (b) **G1** gel phase crystallizations in (i) 1-butanol, (ii) ethanol, and (iii) nitromethane and (iv) cyclohexanone, respectively.

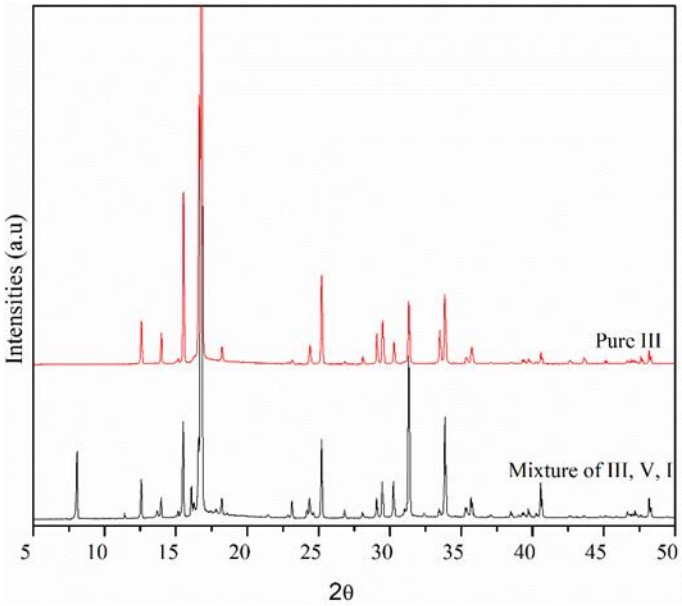

Figure 4 PXRD patterns of BAR only polymorph III obtained inside the gel **G1** in 1-butanol and the mixture of polymorphs obtained from solution crystallization from 1-butanol

Thalidomide Crystallization

(±)Thalidomide has very low solubility in most organic solvents and is practically insoluble in alcohols. So, the crystallization of this drug was restricted to nitromethane, 1,4-dioxane, nitrobenzene and cyclohexanone. To our knowledge concomitant polymorphism of THL has not previously been documented in the literature. Packing energy calculations were undertaken using Mercury 4.2.0[48] for the crystal structures (THALID11-12) deposited in the Cambridge Structural Database and demonstrated comparable packing energies for polymorphs α (–150.6 kJ mol^{-1}) and β (–156.9 kJ mol^{-1}). Interestingly, the two polymorphs crystallize concomitantly upon solution crystallization from nitromethane at concentration 20 mg/mL (Figure 5a). From the solution crystallization in nitromethane, large plate and small needle-shaped crystals were observed. The plate and needle-shaped crystals were characterized by FT-IR spectroscopy, PXRD, and unit cell parameter determination and confirmed as the α and β forms, respectively.[35] The polymorphs can be easily distinguished by comparison of their FT-IR spectra in which the α polymorph exhibits

N-H stretching modes at 3193 and 3098 cm^{-1} while the β polymorph exhibits peaks at 3278 and 3111 cm^{-1} as shown in Figure 6. Crystallization of THL in nitromethane **G1** gels prevents this concomitant crystallization, such that only kinetic form α is formed (Figure 5b). To confirm the phase purity of the crystals obtained inside the gel the PXRD pattern was compared with that simulated from the single-crystal structure and they were found to be in an exact match (see ESI Figure S9).

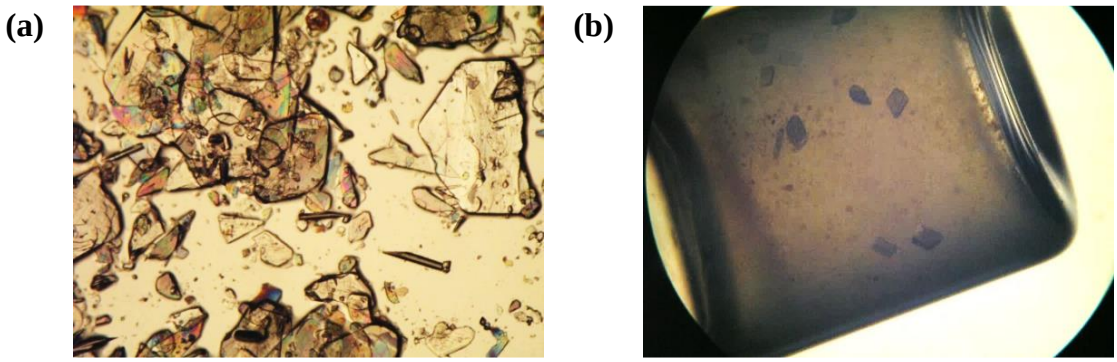

Figure 5 (a) Concomitant crystals plate (α) and needle (β) of THL obtained from solvent evaporation in nitromethane and (b) crystals of only α grown inside the **G1** gel in nitromethane.

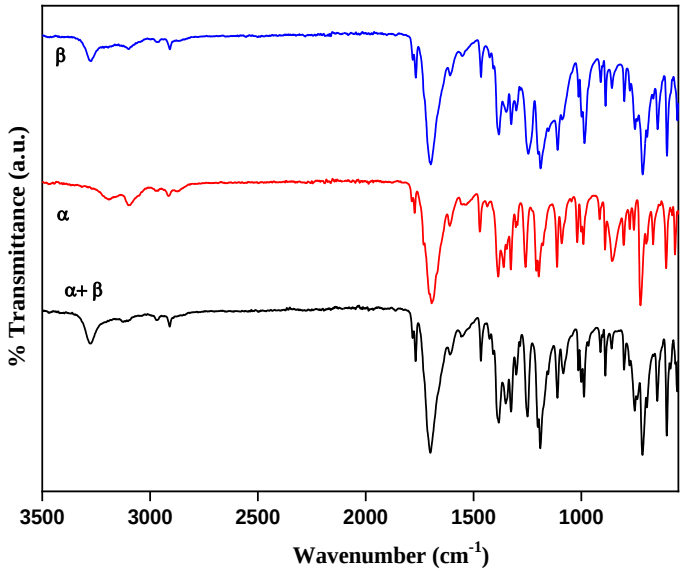

Figure 6 FT-IR spectra comparisons of THL polymorphs α grown inside the gel (red) and concomitant crystals of α and β of THL obtained from solvent evaporation (black) in nitromethane.

The FT-IR spectrum of the β polymorph of THL was obtained by manually separating the crystals (blue).

Under comparable conditions no substantial changes in polymorphic outcome were observed between gel phase (**G1**) and solution phase crystallization by slow cooling in nitrobenzene, 1,4-dioxane and cyclohexanone. However, the gel phase method resulted in a habit change with comparatively larger crystals being formed in the gels compared to solution crystallization in 1,4-dioxane (Table 3).

Table 3 Comparison of crystallization outcome from solution and Gel crystallization of THL

Solvent	**Crystal forms in pure solvent**	**Crystal forms from gel G1**	**Crystal forms from gel G2**	**Crystal forms from G3 gel**
Nitromethane	α and β	α	No gel	Gel not stable
1,4-dioxane	α	α*	No gel	No gel
Cyclohexanone	No crystals	α*	No gel	No gel
Nitrobenzene	No crystals	α†	α†	No crystals

*large needles, †very small crystals

Conclusions

Three new bis(urea) based drug mimetic molecular organogelators were synthesized by the reaction of (±)aminoglutethimide with different diisocyanates. Rheological analysis and SEM images confirm that all three form supramolecular gels with the ethyl-substituted diphenylmethane gelator **G1** being by far the most versatile, consistent with previous.[4,17] The gelators were used as a crystallization media for crystallization of imide containing drugs barbital and (±)-thalidomide. While solution crystallization of BAR in many solvents gave rise to concomitant mixtures, gel phase crystallization using these novel gelators exhibited high selectivity towards the kinetic form

273 III polymorph of barbital. Similarly, in the case of THL, gels of **G1** selectively crystallize the
274 kinetic α form while concomitant mixtures of forms α and β were obtained using solution
275 crystallization methods. It is speculated that the local order of the gel fibers may provide a
276 preferred nucleation site for certain forms and sufficiently favor their crystallization to avoid
277 concomitant crystallization. The use of non-mimetic gelators did not prevent concomitant
278 crystallizations. This indicates that the viscous gel media is not primarily responsible for favoring
279 the kinetic forms. Thus, the use of drug-mimetic gelators is necessary to prevent the concomitant
280 crystallization of BAR and THL. This work demonstrates a promising route to preventing
281 concomitant crystallization in other systems.
282

283 **Experimental**

284 ***Materials and Methods***

285 All the chemicals used were brought from standard commercial sources and were used as such
286 without further purification. (±)-aminoglutethimide was purchased from TCI. The isocyanates
287 were purchased from Sigma Aldrich. All solvents of HPLC grade, triethylamine, and chloroform
288 used in the experiments were purchased from Merck.

289 FTIR spectra of the gelators and the obtained polymorphic form of the drug BAR and THL were
290 recorded in the frequency range of 600–4000 cm^{-1} in a Perkin Elmer Spectrum 100 ATR
291 instrument. Powder diffraction patterns were recorded on a PANalytical Empyrean diffractometer
292 using Cu Kα radiation (λ = 1.54Å), tube voltage of 40kV and 40mA current. Intensities were
293 measured from 5° to 50° 2θ with 0.04 rad. Soller silts and an incident beam divergent slit of 1/8°,
294 antiscatter slit of 1/4° and diffracted beam anti-scatter slit of 7.5mm (PIXcel). All NMR spectra
295 were recorded using a Varian Mercury 400 (^{1}H: 400 MHz; ^{13}C: 100 MHz) spectrometer at room

temperature using deuterated solvent DMSO-d_6. Mass spectra of the compounds were collected using a Thermo-Finnigan LTQ FT mass spectrophotometer. Samples were dissolved in methanol and mass spectra were collected in positive electron spray (ES) mode in the case of **G2** and **G3**, whereas matrix-assisted laser desorption/ionization (MALDI) was used for **G1**. Elemental analysis is performed by using an Exeter Analytical Inc. CE-400 elemental analyzer. Typical sample size 5-7 mg was used to calculate the C, H and N percentage of the prepared compounds. Rheological experiments were performed using advanced rheometer AR 2000 from TA Instruments. The rheometer was equipped with a chiller (Julabo C). Stainless steel 20 mm plain plate geometry was used to perform the experiments. Samples of the gels were prepared in different concentration using different solvents in 7 mL glass *via*ls. The obtained gels were transferred on to the center of the plate of the rheometer using a spatula. The strain sweep measurements were performed to estimate the strain at a constant stress of 10 Pa. Next, frequency sweep measurements and time sweep measurements were performed in the range 0.1 to 4000 Pa. SEM images were obtained on a Hitachi S-5200 field emission scanning microscope. The samples were prepared by applying directly to silicon wafer chips (Agar Scientific) using a stick. Then the samples were kept in vacuum for slow evaporation of solvents. All three samples were coated with 2 nm of Pt and were imaged at 3 KeV and 0.34 nA.

Characterization of gelators

See ESI for details of gelator synthesis.

Gelator ***G1***: Yield = 0.378 g, 0.46 mmol, 85%, MP > 300 ºC. FT-IR: 3320 (N–H), 1692 (C=O), 1650 ($N–H_{bend}$) cm^{-1}; ^{1}H-NMR (DMSO-d_6, 400MHz) δ: 0.75 (t, J = 7.6 Hz, 6H, $-CH_3$) 1.10 (t, J = 8.0 Hz, 12H, $-CH_3$), 1.75-1.87 (m, 4H, $-CH_2$), 2.08–2.19 (m, 4H, $-CH_2$), 2.31–2.46 (m, 4H, -

319 CH_2) 2.51–2.55 (m, 8H, -CH_2), 3.85 (s, 2H, -CH_2), 6.99 (s, 4H, H-Ph), 7.16 (d, *J* = 8.0 Hz, 4H, H-
320 Ph), 7.43 (d, *J* = 8.0 Hz, 4H, H-Ph), 7.56 (s, 2H, NH), 8.82 (s, 2H, NH), 10.83 (s, 2H, NH).^{13}C{^{1}H}-
321 NMR (DMSO-d_6, 100 MHz): δ 176.3, 173.2, 154.3, 142.3, 140.1, 139.7, 132.6, 132.2, 127.0,
322 126.7, 118.2, 50.0, 32.6, 29.5, 26.4, 24.9, 15.1 and 9.3 ppm. MALDI-TOF MS calc. for M+H
323 828.02, experimental 828.00. Elemental analysis: Calc. (%) C, 71.20; H, 7.07; N, 10.03; found.
324 (%) C, 71.18; H, 7.11; and N, 10.03.

325 *Gelator* ***G2***: Yield= 0.346 g, 0.48 mmol, 90%, MP > 300 ºC. FTIR: 3337 (N–H), 1691 (C=O),
326 1650 (N–$H_{bending}$) cm^{-1}; ^{1}H-NMR (DMSO-d_6, 400MHz) δ: 0.75 (t, *J* = 7.4 Hz, 6H, -CH_3), 1.77–
327 1.84 (m, 4H, -CH_2), 2.09-2.17 (m, 4H, -CH_2), 2.31–2.47 (m, 4H, -CH_2), 3.81 (s, 2H, -CH_2), 7.11
328 (d, *J* = 8.0 Hz, 4H, H-Ph), 7.18 (d, *J* = 8.0 Hz, 4H, H-Ph), 7.34 (d, *J* = 8.0 Hz, 4H, H-Ph), 7.43 (d,
329 *J* = 8.0 Hz, 4H, H-Ph), 8.57 (s, 2H, NH), 8.65 (s, 2H, NH), 10.83 (s, 2H, NH). ^{13}C{^{1}H}-NMR:
330 (DMSO-d_6, 100 MHz): δ176.3, 173.2, 152.9, 139.1, 137.9, 135.5, 133.1, 129.3, 127.1, 118.84,
331 118.8, 50.1, 32.6, 29.6, 26.4, and 9.3. MS calculated for M+2H is 357.16, experimental 357.39.
332 Elemental analysis: Calc. (%) C, 68.89; H, 5.92; N, 11.76, found (%): C, 68.29; H, 5.81; and N,
333 11.65.
334

335 *Gelator* ***G3***: Yield= 0.329 g, 0.47 mmol, 87%, MP > 300 ºC. FT-IR: 3341 (N–H), 1695 (C=O),
336 1641 (N–$H_{bending}$) cm^{-1}. ^{1}H-NMR (DMSO-d_6, 400MHz) δ: 0.74 (t, *J* = 8.0 Hz, 6H, -CH_3), 1.59 (s,
337 12H, -CH_3), 1.77–1.82 (m, 4H, -CH_2), 2.06–2.16 (m, 4H, -CH_2), 2.28–2.43 (m, 4H, -CH_2), 6.54
338 (s, 2H, NH), 7.10 (d, *J* = 8 Hz, 4H, H-Ph), 7.23 (s, 4H, H-Ph), 7.31 (d, *J* = 8.0 Hz, 4H, H-Ph), 8.45
339 (s, 2H, NH), 10.81 (s, 2H, NH).^{13}C{^{1}H}-NMR: (DMSO-d_6, 100 MHz): δ 176.3, 173.2, 154.8,
340 148.3, 139.9, 132.2, 128.0, 126.9, 122.9, 121.7, 118.1, 55.0, 50.0, 46.1, 32.6, 30.2, 29.5, 26.4, 12.1,

341 and 9.3. MS calculated for M+H is 709.36, experimental 709.55. Elemental analysis: Calc. (%):
342 C, 67.78; H, 6.83; N, 11.86; found (%): C, 67.39; H, 6.62; and N, 11.56
343
344 ***Gel Screening***
345 Gel screening was carried out at a concentration of 2 % (w/v). Samples were dissolved in 0.5
346 mL of the relevant solvent through gentle heating close to the boiling temperature followed by
347 sonication for 1 min. Gels formation was generally observed within a few minutes but in some
348 case, it requires several hours.
349
350 ***Solution and Gel Phase Recrystallization***
351 Solution crystallizations were performed by the heating of a saturated solution of either BAR or
352 THL until completely dissolved. The solutions were left to cool slowly in a heating block. These
353 were carried out in parallel with gel-phase crystallizations under the same conditions, but in which
354 the heated solution was used to dissolve the gelator. Then the solutions were also left to cool slowly
355 in the heating blocks. Typically gels formed in a few minutes and crystals formed over a matter of
356 hours or days.
357
358 ***Crystal Form Characterisation***
359 Crystals obtained from the solution and gel phase crystallisation experiments were characterized
360 using single crystal x-ray diffraction, XRPD, DSC and microscopic technique.
361
362 ***Supporting Information***

363 Further gelator characterization as well as FT-IR, rheological and XPRD data and Hirshfeld
364 surface analysis available in the electronic supporting information.
365

366 **Acknowledgements**

367 We thank Dr Dmitry S. Yufit and Andrei S. Batsanov for help with unit cell determinations. We
368 are grateful to the Engineering and Physical Sciences Research Council (EP/R013373/1) and
369 Science Engineering and Research Board, India (CRG/2019/004946) for funding and
370 Commonwealth Scholarships Commission for a Split-Site Doctoral Fellowship (to BS). The
371 authors declare no competing financial interest.

372 **References**

373 (1) Osada, Y.; Khokhlov, A. R. *Polymer Gels and Networks*; Marcel Dekker, 2002.
374 (2) Terech, P.; Weiss, R. G. Low Molecular Mass Gelators of Organic Liquids and the
375 Properties of Their Gels. *Chem. Rev.* **1997**, *97*, 3133–3160.
376 (3) Steed, J. W. Supramolecular Gel Chemistry: Developments over the Last Decade. *Chem.*
377 *Commun.* **2011**, *47*, 1379–1383.
378 (4) Steed, J. W. Anion-Tuned Supramolecular Gels: A Natural Evolution from Urea
379 Supramolecular Chemistry. *Chem. Soc. Rev.* **2010**, *39*, 3686–3699.
380 (5) Sangeetha, N. M.; Maitra, U. Supramolecular Gels: Functions and Uses. *Chem. Soc. Rev.*
381 **2005**, *34*, 821–836.
382 (6) Das, D.; Kar, T.; Das, P. K. Gel-Nanocomposites: Materials with Promising Applications.
383 *Soft Matter* **2012**, *8*, 2348–2365.
384 (7) Miao, R.; Peng, J.; Fang, Y. Molecular Gels as Intermediates in the Synthesis of Porous
385 Materials and Fluorescent Films: Concepts and Applications. *Langmuir* **2017**, *33*, 10419–

386 10428.

387 (8) Babu, S. S.; Praveen, V. K.; Ajayaghosh, A. Functional π-Gelators and Their Applications.
388 *Chem. Rev.* **2014**, *114*, 1973–2129.

389 (9) Hirst, A. R.; Escuder, B.; Miravet, J. F.; Smith, D. K. High-Tech Applications of Self-
390 Assembling Supramolecular Nanostructured Gel-Phase Materials: From Regenerative
391 Medicine to Electronic Devices. *Angew. Chem. Int. Ed.* **2008**, *47*, 8002–8018.

392 (10) Serban, B.; Stipe, K.; Alverson, J.; Johnston, E.; Priestley, N.; Serban, M. A Controlled
393 Antibiotic Release System for the Development of Single-Application Otitis Externa
394 Therapeutics. *Gels* **2017**, *3*, 19.

395 (11) Foster, J. A.; Piepenbrock, M. O. M.; Lloyd, G. O.; Clarke, N.; Howard, J. A. K.; Steed, J.
396 W. Anion-Switchable Supramolecular Gels for Controlling Pharmaceutical Crystal Growth.
397 *Nat. Chem.* **2010**, *2*, 1037–1043.

398 (12) Dastidar, P. Supramolecular Gelling Agents: Can They Be Designed? *Chem. Soc. Rev.*
399 **2008**, *37*, 2699–2715.

400 (13) Hirst, A. R., Coates, I. A., Boucheteau, T. R., Miravet, J. F., Escuder, B., Castelletto, V.,
401 Hamley, I. W., and Smith, D. K. Low-Molecular-Weight Gelators: Elucidating the
402 Principles of Gelation Based on Gelator Solubility and a Cooperative Self-Assembly Model.
403 *J. Am. Chem. Soc.* **2008**, *130*, 9113–9121.

404 (14) Zhu, G.; Dordick, J. S. Solvent Effect on Organogel Formation by Low Molecular Weight
405 Molecules. *Chem. Mater.* **2006**, *18*, 5988–5995.

406 (15) Mulvee, M.; Vasiljevic, N.; Mann, S.; Patil, A. J. Construction of Supramolecular
407 Hydrogels Using Photo-Generated Nitric Oxide Radicals. *Soft Matter* **2018**, *14*, 5950–5954.

408 (16) Foster, J. A., Damodaran, K. K., Maurin, A., Day, G. M., Thompson, H. P., Cameron, G.

409 J., Bernal, J. C., and Steed, J. W. Pharmaceutical Polymorph Control in a Drug-Mimetic
410 Supramolecular Gel. *Chem. Sci.* **2016**, *8*, 78–84.
411 (17) Kumar, D. K.; Steed, J. W. Supramolecular Gel Phase Crystallization: Orthogonal Self-
412 Assembly under Non-Equilibrium Conditions. *Chem. Soc. Rev.* **2014**, *43*, 2080–2088.
413 (18) Llinàs, A.; Goodman, J. M. Polymorph control: past, present and future. *Drug Discov.*
414 *Today.* **2008**, *13*, 198−210.
415 (19) Bora, P.; Saikia, B.; Sarma, B. Oriented Crystallization on Organic Monolayers to Control
416 Concomitant Polymorphism. *Chem. Eur. J.* **2020**, *26*, 699–710.
417 (20) Su, C. S.; Liao, C. Y.; Jheng, W. De. Particle Size Control and Crystal Habit Modification
418 of Phenacetin Using Ultrasonic Crystallization. *Chem. Eng. Technol.* **2015**, *38*, 181–186.
419 (21) Trask, A. V. An Overview of Pharmaceutical Cocrystals as Intellectual Property. *Mol.*
420 *Pharm.* **2007**, *4*, 301–309.
421 (22) Sugiyama, T.; Masuhara, H. Laser-Induced Crystallization and Crystal Growth. *Chem.*
422 *Asian J.* **2011**, *6*, 2878–2889.
423 (23) Chen, J.; Sarma, B.; Evans, J. M. B.; Myerson, A. S. Pharmaceutical Crystallization. *Cryst.*
424 *Growth Des.* **2011**, *11*, 887–895.
425 (24) Tyler, A. R.; Ragbirsingh, R.; McMonagle, C. J.; Waddell, P. G.; Heaps, S. E.; Steed, J. W.;
426 Thaw, P.; Hall, M. J.; Probert, M. R. Encapsulated Nanodroplet Crystallization of Organic-
427 Soluble Small Molecules. *Chem* **2020**, *6*, 1755–1765.
428 (25) Shtukenberg, A. G.; Ward, M. D.; Kahr, B. Crystal Growth with Macromolecular Additives.
429 *Chem. Rev.* **2017**, *117*, 14042–14090.
430 (26) Lévesque, A.; Maris, T.; Wuest, J. D. ROY Reclaims Its Crown: New Ways To Increase
431 Polymorphic Diversity. *J. Am. Chem. Soc.* **2020**. *142*, 11873–11883.

432 (27) Zhang, K.; Fellah, N.; Shtukenberg, A. G.; Fu, X.; Hu, C.; Ward, M. D. Discovery of New
433 Polymorphs of the Tuberculosis Drug Isoniazid. *CrystEngComm* **2020**, *22*, 2705–2708.
434 (28) Duffus, C.; Camp, P. J.; Alexander, A. J. Spatial Control of Crystal Nucleation in Agarose
435 Gel. *J. Am. Chem. Soc.* **2009**, *131*, 11676–11677.
436 (29) Diao, Y.; Whaley, K. E.; Helgeson, M. E.; Woldeyes, M. A.; Doyle, P. S.; Myerson, A. S.;
437 Hatton, T. A.; Trout, B. L. Gel-Induced Selective Crystallization of Polymorphs. *J. Am.*
438 *Chem. Soc.* **2012**, *134*, 673–684.
439 (30) Iuzzolino, L.; McCabe, P.; Price, S. L.; Brandenburg, J. G. Crystal Structure Prediction of
440 Flexible Pharmaceutical-like Molecules: Density Functional Tight-Binding as an
441 Intermediate Optimisation Method and for Free Energy Estimation. *Faraday Discuss.* **2018**,
442 *211*, 275–296.
443 (31) Schneider, E.; Vogt, L.; Tuckerman, M. E.; IUCr. Exploring Polymorphism of Benzene and
444 Naphthalene with Free Energy Based Enhanced Molecular Dynamics. *Acta Crystallogr.*
445 *Sect. B Struct. Sci. Cryst. Eng. Mater.* **2016**, *72*, 542–550.
446 (32) Thompson, H. P. G.; Day, G. M. Which Conformations Make Stable Crystal Structures?
447 Mapping Crystalline Molecular Geometries to the Conformational Energy Landscape.
448 *Chem. Sci.* **2014**, *5*, 3173–3182.
449 (33) Dawn, A.; Andrew, K. S.; Yufit, D. S.; Hong, Y.; Reddy, J. P.; Jones, C. D.; Aguilar, J. A.;
450 Steed, J. W. Supramolecular Gel Control of Cisplatin Crystallization: Identification of a
451 New Solvate Form Using a Cisplatin-Mimetic Gelator. *Cryst. Growth Des.* **2015**, *15*, 4591–
452 4599.
453 (34) Tokunaga, E.; Yamamoto, T.; Ito, E.; Shibata, N. Understanding the Thalidomide Chirality
454 in Biological Processes by the Self-Disproportionation of Enantiomers. *Sci. Rep.* **2018**, *8*,

17131.

(35) Reepmeyer, J. C.; Rhodes, M. O.; Cox, D. C.; Silverton, J. V. Characterization and Crystal Structure of Two Polymorphic Forms of Racemic Thalidomide. *J. Chem. Soc. Perkin Trans. 2* **1994**, *0*, 2063.

(36) Zencirci, N.; Griesser, U. J.; Gelbrich, T.; Apperley, D. C.; Harris, R. K. Crystal Polymorphs of Barbital: News about a Classic Polymorphic System. *Mol. Pharm.* **2014**, *11*, 338–350.

(37) MacDonald, J. C.; Biyikli, K.; Zugic, B.; Ebersole, G.; Allor, J. Nucleation and Growth of Polymorphs of Barbital on Chemically Modified Surfaces in Microfluidic Channels. *Mater. Res. Soc. Symp. Proc.* **2005**, *901*, 110–116.

(38) Bernstein, J.; Davey, R. J.; Henck, J. O. Concomitant Polymorphs. *Angew. Chem. Int. Ed.* **1999**, *38*, 3440–3461.

(39) Munshi, P.; Venugopala, K. N.; Jayashree, B. S.; Guru Row, T. N. Concomitant Polymorphism in 3-Acetylcoumarin: Role of Weak C−H···O and C−H···π Interactions. *Cryst. Growth Des.* **2004**, *4*, 1105–1107.

(40) Jiang, S.; Ter Horst, J. H.; Jansens, P. J. Concomitant Polymorphism of O-Aminobenzoic Acid in Antisolvent Crystallization. *Cryst. Growth Des.* **2008**, *8*, 37–43.

(41) Baral, A.; Basak, S.; Basu, K.; Dehsorkhi, A.; Hamley, I. W.; Banerjee, A. Time-Dependent Gel to Gel Transformation of a Peptide Based Supramolecular Gelator. *Soft Matter* **2015**, *11*, 4944–4951.

(42) Castilla, A. M.; Wallace, M.; Mears, L. L. E.; Draper, E. R.; Doutch, J.; Rogers, S.; Adams, D. J. On the Syneresis of an OPV Functionalised Dipeptide Hydrogel. *Soft Matter* **2016**, *12*, 7848–7854.

(43) Torres-Moya, I.; Saikia, B.; Prieto, P.; Carrillo, J. R.; Steed, J. W. High Thermal Stability,

PH Responsive Organogels of 2H-Benzo[d]1,2,3-Triazole Derivatives as Pharmaceutical Crystallization Media. *CrystEngComm* **2019**, *21*, 2135–2143.

(44) Zuidema, J. M.; Rivet, C. J.; Gilbert, R. J.; Morrison, F. A. A Protocol for Rheological Characterization of Hydrogels for Tissue Engineering Strategies. *J. Biomed. Mater. Res. Part B Appl. Biomater.* **2014**, *102*, 1063–1073.

(45) Guvendiren, M.; Lu, H. D.; Burdick, J. A. Shear-Thinning Hydrogels for Biomedical Applications. *Soft Matter* **2012**, *8*, 260–272.

(46) Gavezzotti, A.; Filippini, G. Geometry of the Intermolecular X-H.Cntdot..Cntdot..Cntdot.Y (X, Y = N, O) Hydrogen Bond and the Calibration of Empirical Hydrogen-Bond Potentials. *J. Phys. Chem.* **1994**, *98*, 4831–4837.

(47) Gavezzotti, A. Are Crystal Structures Predictable? *Acc. Chem. Res.* **1994**, *27*, 309–314.

(48) MacRae, C. F.; Sovago, I.; Cottrell, S. J.; Galek, P. T. A.; McCabe, P.; Pidcock, E.; Platings, M.; Shields, G. P.; Stevens, J. S.; Towler, M.; Wood, P. A. Mercury 4.0: From Visualization to Analysis, Design and Prediction. *J. Appl. Crystallogr.* **2020**, *53*, 226–235.

(49) Groom, C. R.; Bruno, I. J.; Lightfoot, M. P.; Ward, S. C. The Cambridge Structural Database. *Acta Crystallogr. Sect. B Struct. Sci. Cryst. Eng. Mater.* **2016**, *72*, 171–179.

(50) Cayuela, A.; Soriano, M. L.; Kennedy, S. R.; Steed, J. W.; Valcárcel, M. Fluorescent Carbon Quantum Dot Hydrogels for Direct Determination of Silver Ions. *Talanta* **2016**, *151*, 100–105.

(51) Spackman, M. A.; McKinnon, J. J. Fingerprinting Intermolecular Interactions in Molecular Crystals. *CrystEngComm* **2002**, *4*, 378–392.

(52) Velásquez-González, O.; Campos-Escamilla, C.; Flores-Ibarra, A.; Esturau-Escofet, N.; Arreguin-Espinosa, R.; Stojanoff, V.; Cuéllar-Cruz, M.; Moreno, A. Crystal Growth in Gels

from the Mechanisms of Crystal Growth to Control of Polymorphism: New Trends on Theoretical and Experimental Aspects. *Crystals* **2019**, *9*, 443.

Table of Contents Graphic